Measured and Modeled Superficial Flow Profiles in Packed Beds with Liquid Flow

M. Giese, K. Rottschäfer, and D. Vortmeyer
Faculty of Mechanical Engineering, Technische Universität München, Boltzmannstr. 15, 85747 Garching, Germany

Packed bed chemical reactors, adsorbers and heat exchangers are simulated by partial differential equations derived from energy and species balances. To solve these equations, an assumption has to be made with respect to the average flow distribution (superficial flow profile) over the cross section of the tubular packed bed. Commonly plug flow is assumed, although the real flow distributions exhibit near-wall flow maxima due to a higher porosity and the no-slip condition at the wall. To our knowledge, Saunders and Ford (1940) were the first to measure the uneven distribution of flow over the exit cross section of the packing. Since then, their observations have been confirmed by numerous authors employing different experimental techniques. An excellent summary of all this work is found in Ziolkowska and Ziolkowski (1988).

Lerou and Froment (1977) evaluated the effect of different flow profiles on the performance of a wall-cooled chemical reactor. Fairly large differences between longitudinal temperature profiles were observed depending on whether the flow profiles were even or uneven. This work found support by Vortmeyer and coworkers (1980, 1981, 1991). In all cases a better simulation of the experimental results was obtained with unevenly distributed profiles. These findings were also observed by Daszkowski and Eigenberger (1992) and in a recent contribution by Papageorgiou and Froment (1995).

A theory to compute superficial flow profiles within the packing was proposed by Vortmeyer and Schuster (1983). They extended the well-known Brinkman equation by the inertia Ergun pressure-loss term and replaced the constant average porosity $\bar{\epsilon}$ by a porosity function $\epsilon(r)$, where r represents the radial position (m).

The use of artificial flow profiles evaluated above the packed bed in the open tube is open to criticism, because one may argue that the profile over the bed is mainly shaped by the last one or two particle layers and that it is deformed by radial circumferential flow components (Drahos et al., 1982) which develop already within the last two particle layers. Price (1968) prevented this shift to a certain extent by fixing a honeycomb structure on top of the packed bed. In a recent work of Bey and Eigenberger (1997) the structure of the outlet flow is preserved by a monolith.

In the past, the most successful attempts to measure velocities inside the packed bed involved the use of Laser-Doppler-velocimetry with matched refraction indices of fluid and solid. Johnson and Dybbs (1975) and Dybbs and Edwards (1984) applied this method to packed beds consisting of plexiglas spheres. The interest of Northrup et al. (1992) was the nature of flow within the voids of the bed. They obtained important results by the method of particle imaging. McGreavy et al. (1986) measured velocity profiles inside a packed bed having a ratio D/d_p of about 3; because of this ratio, they could find passes for optical access. Another group of authors injected a tracer and analyzed the spreading of the tracer to draw conclusions concerning the flow. Stephenson and Stewart (1986) took photographs of small marker bubbles and found an oscillating flow profile in a packed bed of cylinders, which is included in Figure 5. Other tracers were inserted by Cairns and Prausnitz (1959), Caycik and Gunn (1988) and Lamine et al. (1992).

In summarizing the available literature, one has to conclude that there is strong evidence for the existence of superficial velocity profiles with unevenly distributed flow inside the packed bed. However, due to the small number of actual measurements, the precise nature of the profiles and their dependence on the Reynolds number and particle shape is not known.

Experimental Studies

For the purpose of averaging, a large number of measured axial flow components over a cross section has to be available. Therefore, an automatically controlled apparatus was designed based on Laser-Doppler-velocimetry in a refraction-index matched system. The spheres and other glass components were made from Duranglas (Schott Co.) of high quality to minimize scattering effects due to impurities. The tube with an inner diameter of 80 mm and the container were mounted on a high precision table, which could be moved with an accuracy of ± 0.025 mm in three directions under the control of a computer. A constant temperature was obtained by a heat exchanger integrated in the fluid circuit. The liquid was a mixture of 95% dibutylphtalat and 5% ethyl-alcohol to match the refraction index of $n = 1.473$ at the wavelength of the laser $\lambda = 632.8$ nm at around 24°C. The fine adjustment was achieved by slight temperature regulations and an optical

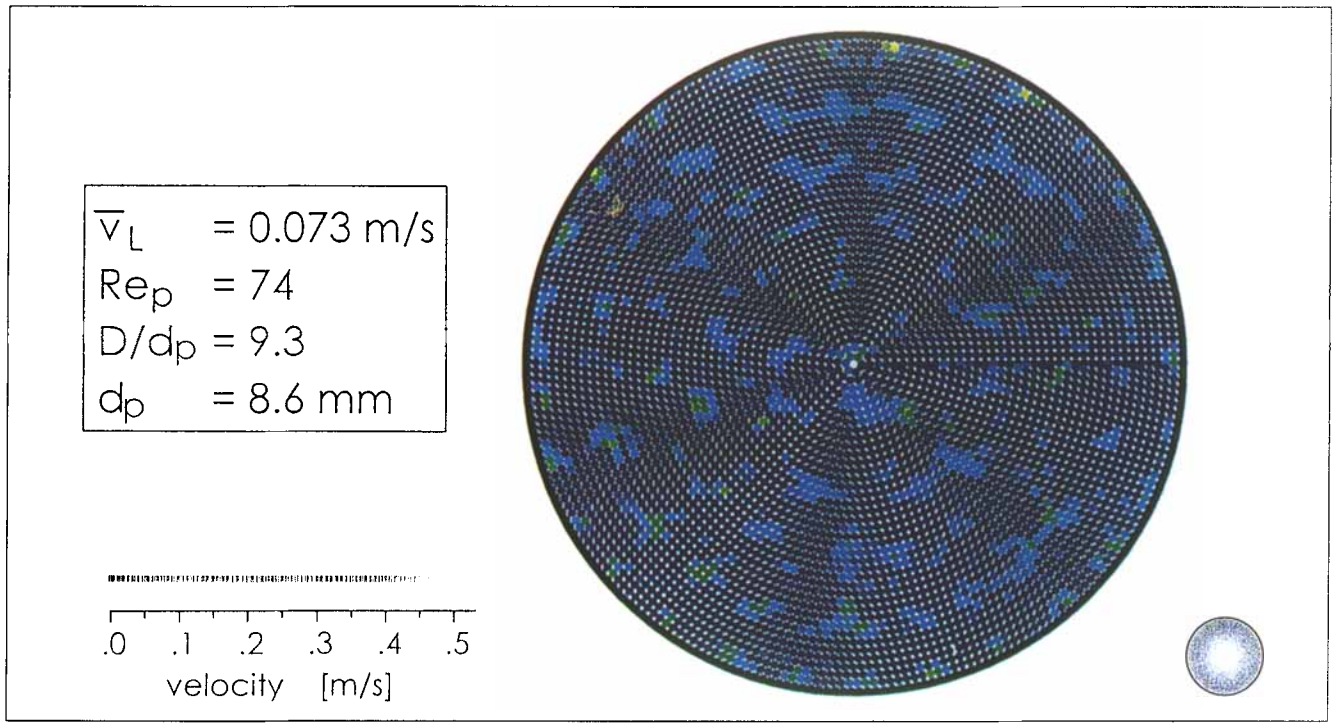

Figure 1. Distribution of local axial flow components measured over a cross section of a tubular packing of spheres at *Re* = 74.

wedge. Best signal quality was obtained with Latex tracer particles in the fluid. At 24°C the density of the fluid was $\rho = 1{,}006.9$ kg/m^3 and its viscosity was $\eta = 8.5 \times 10^{-3}$ N·s/m^2. The closest distance between two measured velocities was 1 mm which means that a grid with a mesh size of 1 mm^2 was spread over the cross section resulting in more than 5,000 samples outside and inside the particles. Naturally, the flow rate within the nonporous particles was measured to be zero. Details on the experimental techniques are found in the dissertation of Rottschäfer (1996).

Usually, the signals were recorded for one second and averaged by the tracker. Averaged local point velocities are plotted in the colored chart of Figure 1 for a packed bed consisting of spheres. As the dark blue color indicates zero velocity, we can identify the spheres close to the wall in an ordered arrangement, which gradually disappears towards the center of the bed. Nevertheless, a second and third row of spheres can clearly be observed.

Although interstitial flow velocities are measured, superficial velocities are obtained by averaging the point velocities at a fixed radius r including zero velocities inside a particle over the circumference. These averaged velocities are plotted in the Figures 3 to 6 for bed of spheres, deformed spheres, cylinders and Raschig-rings and are compared with theoretical predictions. For this purpose, the porosity distributions or porosity functions $\epsilon(r)$ across the tube diameter have to be known also. Instead of relying on literature data, we have measured the porosity distributions in Figure 2 for all particle beds. In this, we followed the method of Ridgway and Tarbuck (1966) with the packed bed contained in a cylindrical drum rotating at high speed around its axis.

In all cases, the volumetric flow rates obtained by integrating the artificial flow profiles were only a few percent (2–5%) lower than the metered ones, which provides a good check for the quality of the flow measurements.

Theoretical interpretation of artificial flow profiles

Vortmeyer and Schuster (1981, 1983) proposed to model flow profiles inside packed beds by the Brinkman equation (1947) to which they added an inertia term for higher flow rates.

$$\frac{\partial p}{\partial z} = -f_1 v - f_2 v^2 + \frac{\eta_{\text{eff}}}{r}\frac{\partial}{\partial r}\left(r\frac{\partial v}{\partial r}\right) \tag{1}$$

The factors f_1 and f_2 were chosen from the Ergun (1952) pressure-loss relation

$$f_1 = 150\frac{(1-\bar{\epsilon})^2}{\bar{\epsilon}^3}\frac{\eta}{d_p^2} \qquad f_2 = 1.75\frac{(1-\bar{\epsilon})}{\bar{\epsilon}^3}\frac{\rho}{d_p} \tag{2}$$

Naturally, it should be noted that other pressure drop factors could also be considered, as, for example, those presented by Molerus (1977).

$$f_1 = \left(\frac{18}{(1-\bar{\epsilon})} + \frac{49.5}{\bar{\epsilon}}\right)\frac{(1-\bar{\epsilon})^2}{\bar{\epsilon}^2}\frac{\eta}{d_p^2} \qquad f_2 = 0.69\frac{(1-\bar{\epsilon})}{\bar{\epsilon}^4}\frac{\rho}{d_p} \tag{3}$$

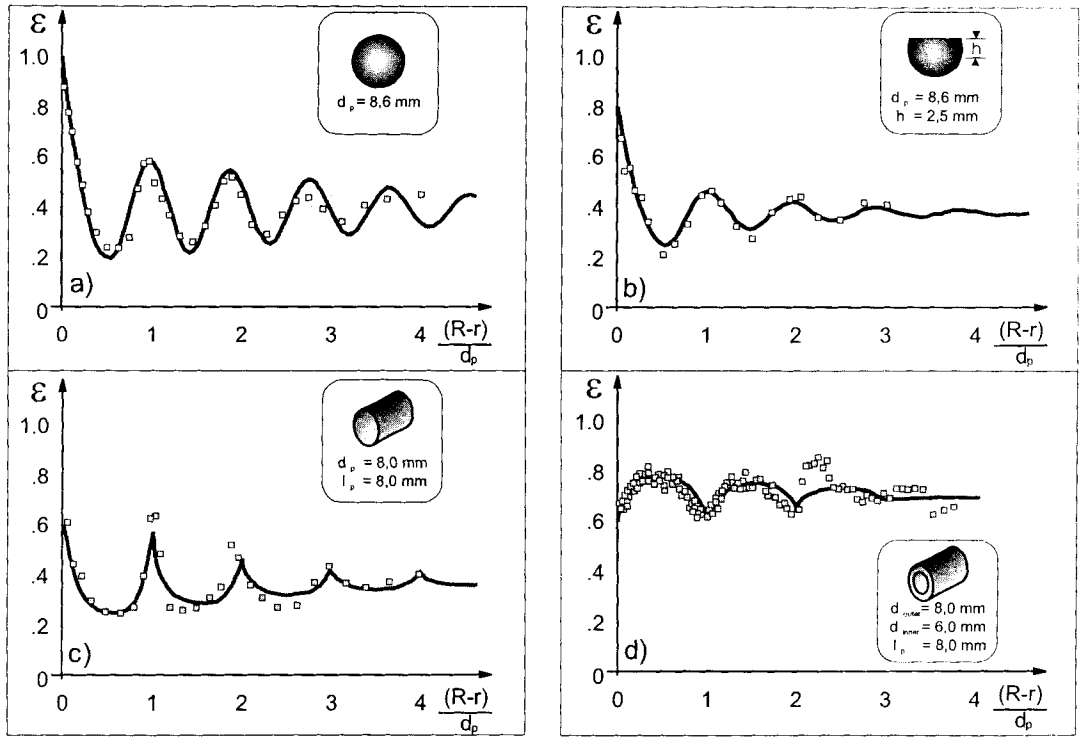

Figure 2. Measured porosity functions for packed beds of spheres (a), deformed spheres (b), cylinders (c), and Raschig-rings (d).

To apply Eq. 1 to the porosity distributions of Figure 2 for the packings under consideration, the average porosities $\bar{\epsilon}$ in f_1 and f_2 were replaced by the measured porosity function $\epsilon(r)$. Equation 1 then becomes

$$\frac{\partial p}{\partial z} = -150\frac{(1-\epsilon(r))^2}{\epsilon(r)^3}\frac{\eta}{d_p^2}v - 1.75\frac{(1-\epsilon(r))}{\epsilon(r)^3}\frac{\rho}{d_p}v^2 + \frac{\eta_{\text{eff}}}{r}\frac{\partial}{\partial r}\left(r\frac{\partial v}{\partial r}\right) \quad (4)$$

This equation was solved under the following boundary conditions

$$r = 0: \qquad \frac{\partial v}{\partial r} = 0 \quad (5)$$

$$r = R: \qquad v = 0 \quad (6)$$

and

$$\dot{V} = \int_0^R 2\pi r v dr \quad (7)$$

The unknown effective viscosity η_{eff} (kg/ms) in Eq. 4 is obtained by fitting theory and experiment. It will be seen later that the influence of η_{eff} is restricted to a region close to the wall only.

Measured and modeled superficial flow profiles

The full body of experimental findings together with the solutions of the extended Brinkman equation model are presented in Figures 3–6. The packing of spheres is shown in Figure 3, deformed spheres in Figure 4, cylinders in Figure 5 and for Raschig-rings in Figure 6.

The radial distribution of artificial flow velocities in Figure 3 for a tubular packed bed of spheres is based on flow measurements within two different cross sections at the Reynolds numbers of $Re_p = 4$, 77, 103 and $Re_p = 532$. The very good agreement between both measured profiles indicates that the averaged flow profiles are constant along the packing if the flow is fully developed. While the scatter of experimental points is low in the outer section of the packed bed, it increases towards the center of the packing due to the lower number of flow measurements.

We observe further that the oscillations of the flow profiles reflect the oscillations of the porosity profile in Figure 2 over the whole cross section. For the nonspherical particles in Figure 4, only two or three maxima can be identified indicating that the state of randomness is reached already at a distance of two or three particle diameters away from the wall.

Cylinders as filling material exhibit a porosity distribution according to Figure 2c with a wall porosity of $\epsilon_w = 0.62$ and point maxima at positions where the distance to the wall corresponds to one or more particle diameters. The measured flow profiles in Figure 5 for three different Reynolds numbers of $Re_p = 136$, 56 and 4 follow the porosity function and are modeled very well by the solutions of the extended Brinkman equation. The dotted line in Figure 5c exhibits an artificial flow profile which was obtained by Stephenson and

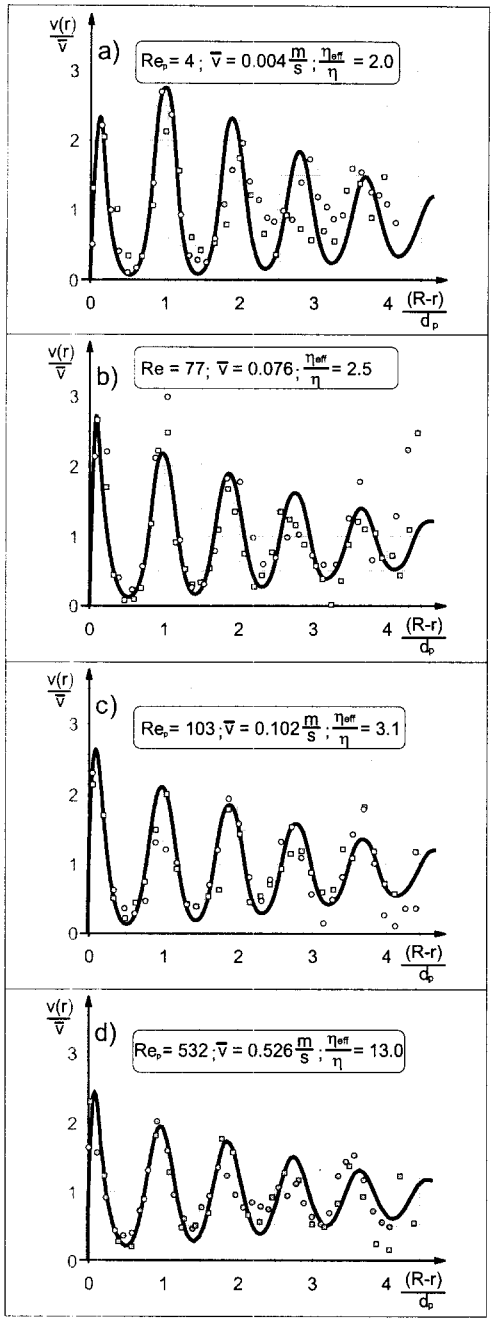

Figure 3. Experimental and modeled (full line) flow distributions within a bed of spheres.

Different symbols represent measurements in different cross sections.

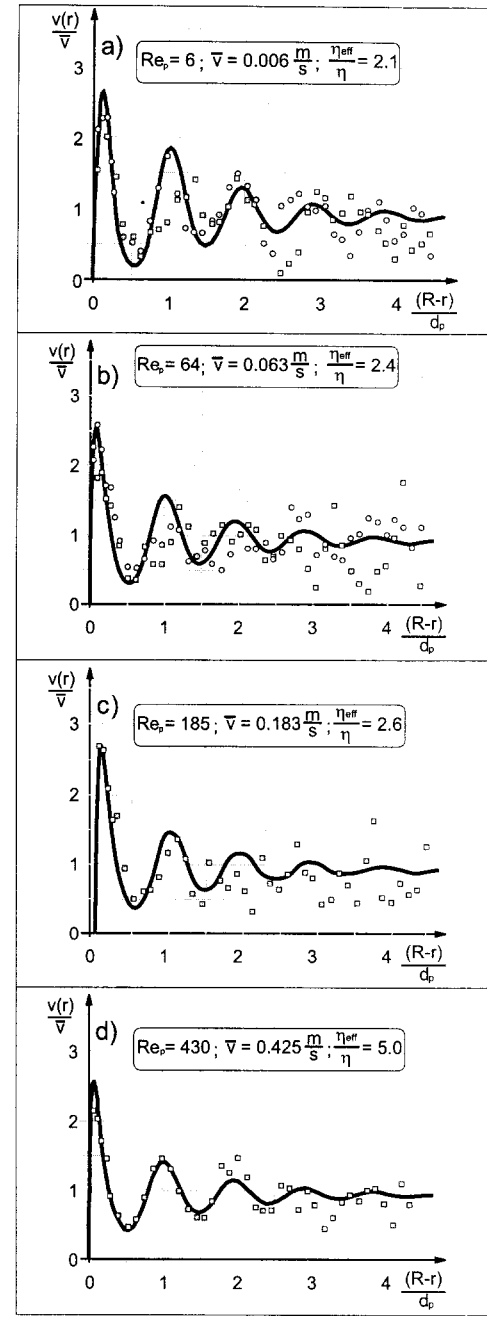

Figure 4. Flow distribution for packings of deformed spheres.

Stewart (1986) for a packed bed of cylinders with $D/d_p = 10.7$ and $5 < Re_p < 280$. The curve is based on axial flow velocities of marker bubbles in a refraction index matched system. The flow maxima and minima follow the course of our results. The effective viscosities in Figure 8 are smaller than those for spheres and deformed spheres.

Some discrepancies between theory and experiment are observed for packed beds of Raschig-rings at Reynolds numbers of 3, 65 and 458 within the near wall region. We believe that these effects are due to the complicated flow structure of the flow around and inside the hollow cylinders.

The influence of the effective viscosity η_{eff} on the solution of the extended Brinkman Eq. 4 is demonstrated in Figure 7c where the flow profiles were calculated for $\eta_{eff}/\eta = 3$, 13 and 30 with the best fit for $\eta_{eff}/\eta = 13$. One observes furthermore that the influence of the effective viscosity is restricted to a region very close to the wall only, as it serves to model the near wall flow maximum.

It is an inherent assumption of our model that the pressure loss relation is locally valid close to the wall up to porosities of $\epsilon_w = 1$ for spheres. However, it is well known that the Ergun-equation should be applied only to bed porosities of $\epsilon = 0.5$. We have therefore also performed calculations for the

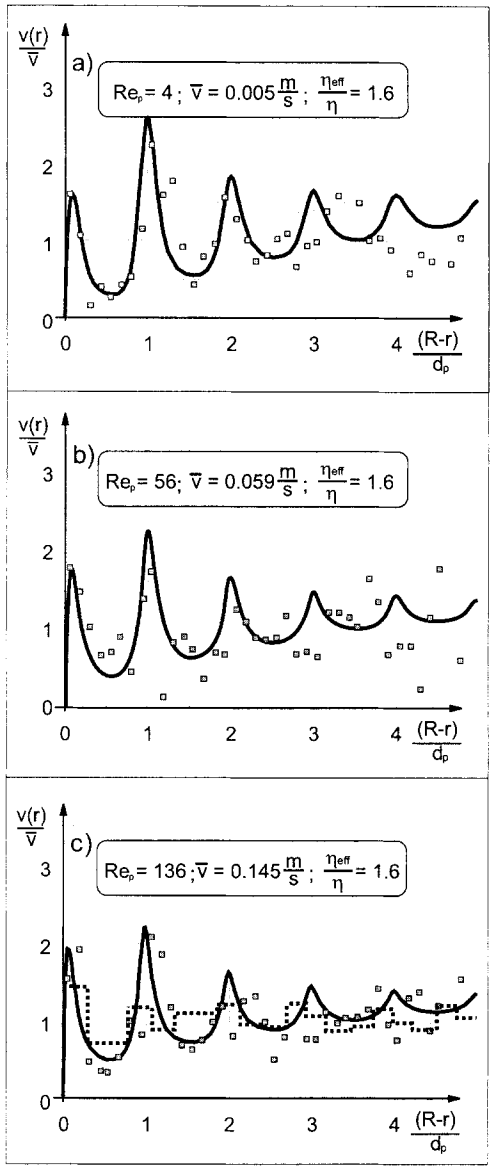

Figure 5. Flow distribution for packings of cylinders.

Dotted line in (c) represents measurements by Stephenson and Stewart (1992).

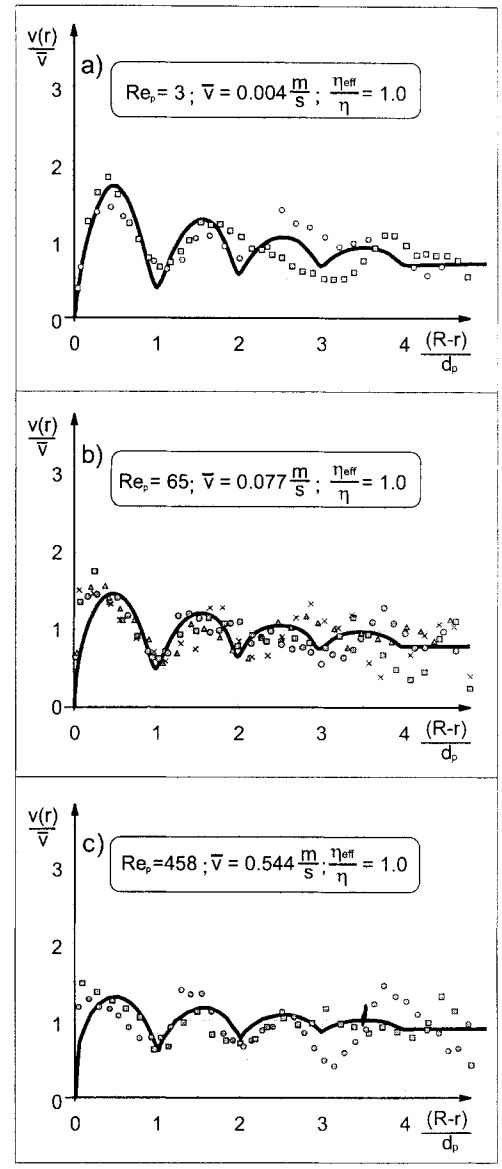

Figure 6. Flow distribution for packings of Raschig rings.

pressure loss relation published by Molerus (1977) with coefficients according to Eq. 3. This relation has the merit to be valid for porosities up to $\epsilon = 0.7$. The best fit with regard to the Molerus equation was obtained for $\eta_{\text{eff}}/\eta = 17$ instead of 13 for the Ergun equation, which can be seen from Figure 7b.

As the pressure loss relations are only valid for a limited range of porosities, it is obvious that the porosity function in the immediate vicinity of the wall has a strong influence on η_{eff}. While the previous computations for spheres are based on $\epsilon_w = 1$ at the wall, one can argue that under flow conditions, there are small fillets of stagnant flow around the contact points between the spheres and the wall, a fact which would reduce the porosity at the tube wall. Therefore, as a matter of interest we have performed calculations with porosity functions for spheres of Figure 2 starting with wall porosities of $\epsilon_w = 0.8$ and 0.9 instead of $\epsilon_w = 1$. For these conditions, best fits in Figure 7a are obtained with $\eta_{\text{eff}}/\eta = 4$ for $\epsilon_w = 0.8$ and $\eta_{\text{eff}}/\eta = 8$ for $\epsilon_w = 0.9$ instead of $\eta_{\text{eff}}/\eta = 13$ for $\epsilon_w = 1$.

Different symbols in one or the other figure correspond to measurements in different cross sections. To obtain best fits by theory, effective viscosities had to be raised for packed beds of spheres and deformed spheres with increasing Reynolds numbers as shown in Figure 8. The nonlinear relation between η_{eff} and Re can be expressed by the empirical correlation

$$\frac{\eta_{\text{eff}}}{\eta} = a \cdot \exp(bRe_p) \tag{8}$$

with

$a = 2.0, \quad b = 3.5 \times 10^{-3}$ for spheres

$a = 2.0, \quad b = 2.0 \times 10^{-3}$ for deformed spheres

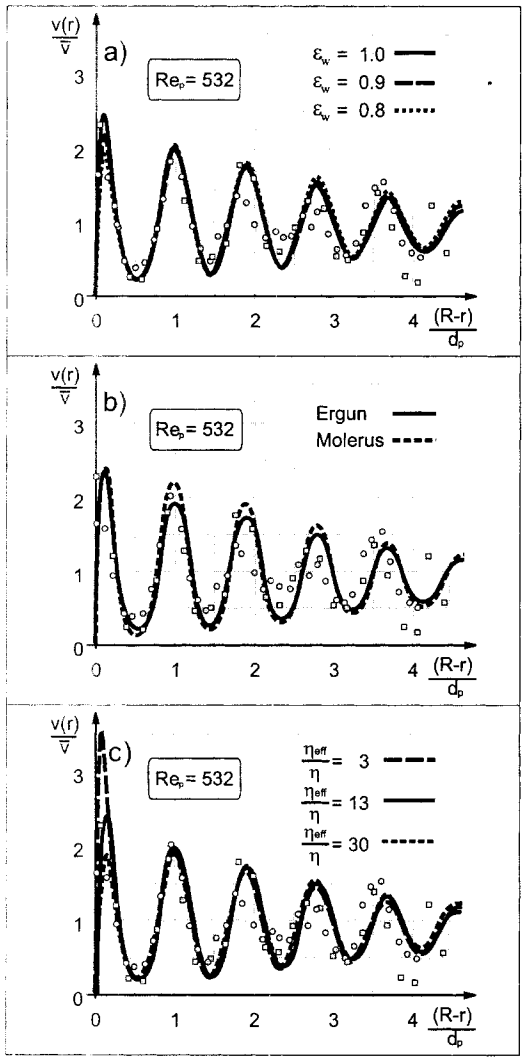

Figure 7. Influence of the effective viscosity (a), of the pressure loss relation (b), and of the wall porosity (c) on the solution of the extended Brinkman equation.

No such effect was observed for packed beds of cylinders and Raschig-rings with effective viscosities independent of the Reynolds number within the experimental range. This different behavior of the effective viscosities is obviously linked to the porosities ϵ_w at the wall with $\epsilon_w = 1$ for spheres and $\epsilon_w = 0.8$ for deformed spheres while beds of cylinders and Raschig-rings exhibit lower values of $\epsilon_w = 0.6$.

Figure 8 also contains an effective viscosity which was evaluated by Givler and Altobelli (1994) for gas flowing through a porous medium with a constant porosity of $\epsilon = 0.972$. The permeability of their presentation was reduced by us to a diameter of an equivalent spherical particle on which the Reynolds number finally was based.

Conclusions

For liquid flow, superficial velocity profiles inside a packed bed were obtained for monodisperse packings of spheres, deformed spheres, cylinders and Raschig-rings by averaging over

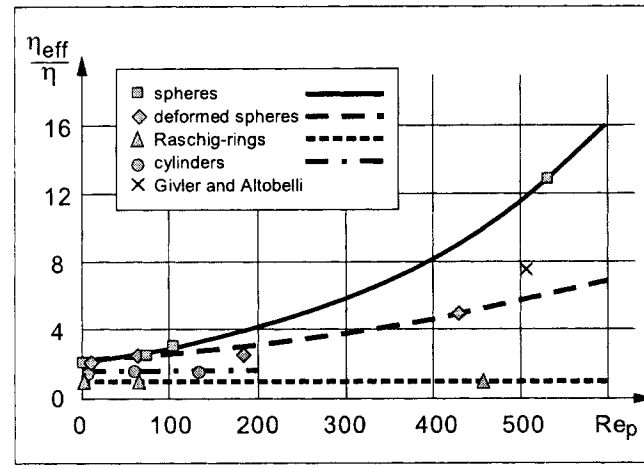

Figure 8. Effective viscosity data depending on particle shape and Reynolds number.

several thousand local measurements of the axial flow components within a cross-section. At fully developed flow, the profiles are constant along the packing except for short inlet and outlet zones of about three particle layer length with either a buildup of the profile at the inlet or a degeneration at the exit of the packed bed. Besides velocity profiles, porosity distribution functions were also evaluated experimentally. These were introduced in the extended Brinkman equation which simulates the fluctuating profiles well if the average porosity $\bar{\epsilon}$ of the packing is replaced by the radial porosity distribution $\epsilon(r)$. The effective viscosity η_{eff} is adjusted to obtain best agreement between measurements and solutions of the Brinkman equation. This effective property, however, influences the flow profile in the very near wall range only, up to approximately a distance of about half the particle diameter. The effective viscosity is found to depend on the porosity data close to the wall, on particle shape, on the Reynolds number, and on the pressure loss relation.

Acknowledgments

Financial support by the Deutsche Forschungsgemeinschaft is gratefully acknowledged.

Notation

d_p = partial diameter, m
D = tube diameter, m
p = pressure, N/m^2
R = tube radius, m
Re_p = Reynolds number ($= \bar{v}\rho d_p/\eta_F$)
$\bar{v}$ = average superficial velocity, m/s
$v(r)$ = superficial velocity, m/s
$\dot{V} = \dot{V} = \pi R^2 \bar{v}$, volume flow rate, m^3/s
z = axial coordinate, m
η = dynamic fluid viscosity, kg/ms
ρ = fluid density, kg/m^3

Literature Cited

Bey, O., and G. Eigenberger, "Fluid Flow through Catalyst Filled Tubes," *Chem. Eng. Sci.*, **52**, 1365 (1997).

Brinkman, H. C., "A Calculation of the Viscous Force Exerted by a Flowing Fluid on a Dense Swarm of Particles," *Appl. Sci. Res.*, **A1**, 27 (1947).

Cairns, E. J., and J. M. Prausnitz, "Velocity Profiles in Packed and Fluidized Beds," *Ind. Eng. Chem.*, **51**(12), 1441 (1959).
Caycik, M., and D. J. Gunn, "True Mean Velocities in the Wall and Buld Regions of the Fixed Beds," *Chem. Eng. Sci.*, **43**(7), 1637 (1988).
Daszkowski, T., and G. Eigenberger, "A Reevaluation of Fluid Flow, Heat Transfer and Chemical Reaction in Catalyst Filled Tubes," *Chem. Eng. Sci.*, **47**, 2245 (1992).
Drahos, J., J. Cermak, I. Ziolkowska, and D. Ziolkowski, "Statistical Analysis of Local Gas Velocities at the Exit from a Packed Bed," *Chem. Eng. J.*, **24**, 71 (1982).
Dybbs, A., and R. V. Edwards, "A New Look at Porous Media Fluid Mechanics—Darcy to Turbulent," *NATO ASI Ser.*, **82**(1), 199 (1995).
Ergun, S., "Fluid Flow through Packed Columns," *Chem. Eng. Proc.*, **48**(2), 89 (1952).
Givler, R. C., and S. A. Altobelli, "A Determination of the Effective Viscosity for the Brinkman-Forchheimer Flow Model," *J. Fluid Mech.*, **258**, 355 (1994).
Johnson, W., A. Dybbs, and R. Edwards, "Measurement of Fluid Velocity inside Porous Media with Laser Anemometer," *Phys. of Fluids*, **18**(7), 913 (1975).
Kalthoff, O., and D. Vortmeyer, "Ignition/Extinction Phenomena in a Wall Cooled Fixed Bed Reactor," *Chem. Eng. Sci.*, **35**, 1637 (1980).
Lamine, A. S., M. T. Colli Serrano, and G. Wild, "Hydrodynamics and Heat Transfer in Packed Beds with Liquid Upflow," *Chem. Eng. and Proc.*, **31**, 385 (1992).
Lerou, J. J., and G. F. Froment, "Velocity, Temperature and Conversion Profiles in Fixed Bed Catalytic Reactors," *Chem. Eng. Sci.*, **32**, 853 (1977).
McGreavy, C., E. A. Foumeny, and K. H. Javed, "Characterization of Transport Properties for Fixed Bed in Terms of Local Bed Structure and Flow Distribution," *Chem. Eng. Sci.*, **41**, 787 (1986).
Molerus, O., "Druckverlustg Leichung für die Durch-strömung von Kugelschüttungen im Laminaren und im Übergangs bereich," *Chem. Eng. Tech.*, **49**, 675 (1977).
Northrup, N. A., T. J. Kulp, and S. M. Angel, "Imaging of Interstitial Velocity Fields and Tracer Distributions in a Refractive Index-Matched Porous Medium," *Heat and Mass Transfer in Porous Media*, **48**, 158 (1992).
Papageorgiou, J. N., and G. F. Froment, "Simulation Models Accounting for Radial Voidage Profiles in Fixed-Bed Reactors," *Chem. Eng. Sci.*, **50**(19), 3043 (1995).
Price, J., "The Distributions of Fluid Velocities for Randomly Packed Beds of Spheres," *Mech. and Chem. Eng. Trans.*, **1**, 7 (1968).
Ridgway, K., and K. J. Tarbuck, "Radial Voidage Variation in Randomly-Packed Beds of Spheres of Different Sizes," *J. Pharm. Pharmac.*, **18**, 168 (1966).
Rottschäfer, K., "Geschwindigkeitsverteilungen in Durchströmten Füllkörperschüttungen," PhD Diss., TU-München (1996).
Saunders, O. A., and H. Ford, "Heat Transfer in the Flow of Gas through a Bed of Solid Particles," *J. of the Iron and Steel Inst.*, **141**, 291 (1940).
Stephenson, J. L., and W. E. Stewart, "Optical Measurements of Porosity and Fluid Motion in Packed Beds," *Chem. Eng. Sci.*, **41**(8), 2161 (1986).
Vortmeyer, D., and E. Haidegger, "Discrimination of Three Approaches to Evaluate Heat Fluxes for Wall-Cooled Fixed Bed Chemical Reactors," *Chem. Eng. Sci.*, **46**(10), 2651 (1991).
Vortmeyer, D., and J. Schuster, "Evaluation of Steady Flow Profiles in Rectangular and Circular Packed Beds by a Variational Method," *Chem. Eng. Sci.*, **38**(10), 1691 (1983).
Vortmeyer, D., and R. P. Winter, "Impact of Porosity and Velocity Distribution on the Theoretical Prediction of Fixed Bed Chemical Reactor Performance," in *ACS Symp. Ser. 196, Chem. Reac. Eng.*, Boston, p. 49 (1981).
Ziolkowska, I., and D. Ziolkowski, "Fluid Flow Inside Packed Beds," *Chem. Eng. Sci.*, **23**, 137 (1988).

Manuscript received Mar. 19, 1997, and revision received Oct. 2, 1997.